Helical Interactions in the HIV-1 gp41 Core Reveal Structural Basis for the Inhibitory Activity of gp41 Peptides[†,‡]

Wei Shu,[§] Jie Liu,[§] Hong Ji,[§] Lin Radigen,[||] Shibo Jiang,[||] and Min Lu*[,§]

Department of Biochemistry, Weill Medical College of Cornell University, 1300 York Avenue, New York, New York 10021, and Lindsley F. Kimball Research Institute, New York Blood Center, New York, New York 10021

Received September 20, 1999; Revised Manuscript Received November 30, 1999

ABSTRACT: The HIV-1 gp41 envelope protein mediates membrane fusion that leads to virus entry into the cell. The core structure of fusion-active gp41 is a six-helix bundle in which an N-terminal three-stranded coiled coil is surrounded by a sheath of antiparallel C-terminal helices. A conserved glutamine (Gln 652) buried in this helical interface replaced by leucine increases HIV-1 infectivity. To define the basis for this enhanced membrane fusion activity, we investigate the role of the Gln 652 to Leu substitution on the conformation, stability, and biological activity of the N34(L6)C28 model of the gp41 ectodomain core. The 2.0 Å resolution crystal structure of the mutant molecule shows that the Leu 652 side chains make prominent contacts with hydrophobic grooves on the surface of the central coiled coil. The Gln 652 to Leu mutation leads to a marginal stabilization of the six-helix bundle by −0.8 kcal/mol, evaluated from thermal unfolding experiments. Strikingly, the mutant N34(L6)C28 peptide is a potent inhibitor of HIV-1 infection, with 10-fold greater activity than the wild-type molecule. This inhibitory potency can be traced to the corresponding C-terminal mutant peptide that likely has greater potential to interact with the coiled-coil trimer. These results provide strong evidence that conserved interhelical packing interactions in the gp41 core are important determinants of HIV-1 entry and its inhibition. These interactions also offer a test-bed for the development of more potent analogues of gp41 peptide inhibitors.

The human immunodeficiency virus type 1 (HIV-1)[1] enters cells by the envelope protein-mediated membrane fusion process that allows invasion of the infectious viral genome. The envelope glycoprotein of HIV-1 consists of a complex of the surface subunit gp120 and the transmembrane subunit gp41, which are generated through proteolytic cleavage of the polypeptide precursor gp160 (reviewed in refs *1*−*3*). The envelope glycoprotein is displayed on the lipid bilayer of the virion as well as on the plasma membrane of infected cells. gp120 is responsible for binding to the CD4 glycoprotein and a chemokine receptor on the T cell surface (*4*, *5*). Subsequently, gp41 undergoes conformational changes that facilitate membrane fusion between virus and target cell during infection, and between infected cells and uninfected cells during multinucleated giant cell (syncytium) formation (*3*). This receptor binding-promoted fusion activation is thought to involve conformational changes in the envelope protein complex from a native (nonfusogenic) to a fusion-active (fusogenic) state (for a recent review, see ref *6*). The control of this fusion activation process involving multiple protein interactions is central to the complex biology of HIV-1 entry and its inhibition.

The gp41 molecule contains several characteristic features within its ectodomain. Toward its amino terminus is the hydrophobic, glycine-rich sequence referred to as the fusion peptide, which is thought to insert into the bilayer of the target membrane at an early step of the fusion process (*7*−*11*). This fusion peptide region is followed by two regions that exhibit a 4−3 repeat of hydrophobic amino acids with the potential to form α-helical coiled-coil structures (*12*−*14*). The N (amino)-terminal heptad repeat is located adjacent to the fusion peptide, while the C (carboxyl)-terminal repeat precedes the transmembrane segment. Between these heptad-repeat regions is a disulfide-bonded loop region. Limited proteolysis studies identified a stable core of the gp41 ectodomain, in which the two heptad-repeat regions form a trimer of antiparallel dimers (*15*, *16*). The X-ray crystal structure of this core reveals that three N-terminal helices form a central, three-stranded coiled coil, whereas three C-terminal helices pack in an antiparallel orientation into three hydrophobic grooves on the surface of this coiled-coil trimer (*17*−*19*). We have previously shown that a monoclonal antibody specifically recognizing this six-helix bundle binds to the surface of HIV-1 infected cells only after interaction of the envelope protein complex with soluble CD4 (*20*). This finding provides direct evidence for the notion that the gp41 ectodomain core represents the fusion-active conformation of the HIV-1 envelope protein

[†] This work was supported by National Institutes of Health Grants AI42693 to S.J. and AI42382 to M.L. and by the New York City Council Speaker's Fund for Biomedical Research to M.L.

[‡] The refined coordinates have been deposited in the Protein Data Bank with accession number 1DLB.

* To whom correspondence should be addressed. Phone: (212) 746-6562. Fax: (212) 746-8875. E-mail: mlu@mail.med.cornell.edu.

[§] Weill Medical College of Cornell University.

[||] Lindsley F. Kimball Research Institute.

[1] Abbreviations: HIV-1, human immunodeficiency virus type 1; $[\theta]_{222}$, molar ellipticity at 222 nm; CD, circular dichroism; HPLC, high-performance liquid chromatography; LB, Luria-Bertani; T_m, midpoint of thermal denaturation; GdmCl, guanidinium hydrochloride; IPTG, isopropylthio-β-galactoside; PBS, neutral pH phosphate-buffered saline; PDB, Protein Data Bank; rms, root-mean-square; BCECF-AM, 2′,7′-bis-(2-carboxyethyl)-5-(and-6)-carboxyfluorescein-acetoxymethyl ester; CPE, HIV-1_{IIIB}-mediated cytopathic effect.

10.1021/bi9921687 CCC: $19.00
Published on Web 02/15/2000

(*15*, *17*−*19*). In addition, the six-helix bundle appears to play a direct role in membrane fusion because the folding and stability of the gp41 core in vitro correlate well with severity of the in vivo phenotypes observed in cells expressing engineered HIV-1 envelope protein variants (*21*, *22*).

The current model for gp41-mediated membrane fusion is that a conformational change and subsequent antiparallel association of α-helices in the gp41 ectodomain place the viral and cellular membranes into close proximity for fusion (*18*, *23*, *24*). According to this model, packing interactions between the central coiled-coil trimer and the C-terminal helix are critical for membrane fusion. In the crystal structure of the gp41 core, Gln 652 and Asn 656 at ***a*** and ***d*** positions of the C-terminal helix pack against the N-terminal coiled coil (*17*−*19*). When Gln 652 was replaced by leucine, the mutant virus is more infectious than the wild-type virus (*25*). In contrast, a leucine substitution for Asn 656 abolishes infectivity and membrane fusion (*25*). Thus, the buried face of the C-terminal helix and its packing interactions with the N-terminal coiled coil appear to control the key process of HIV-1 entry. These conserved packing interactions also play a major role in the ability of synthetic peptides corresponding to the C-terminal helix to inhibit HIV-1 infection (*26*, *27*). The available evidence suggests that these peptide inhibitors act in a dominant-negative manner by binding to the N-terminal coiled coil of gp41 (*15*, *17*−*19*, *24*, *26*−*32*). In addition, recent studies indicate that the structural and mechanistic basis of helical interactions is conserved in many viral membrane fusion proteins (e.g., refs *33* and *34*).

Here we use the recombinant N34(L6)C28 model (*21*) to characterize the effects of the Gln 652 to Leu mutation on the structure and biological activity of the gp41 ectodomain core. Circular dichroism and sedimentation equilibrium measurements indicate that the Q652L mutant forms a trimeric helical structure. The stability of the Q652L trimer increases by 0.8 kcal/mol, relative to the wild-type complex. The X-ray crystal structure of Q652L at 2.0 Å resolution reveals that the mutant sequence is accommodated in the six-helix bundle by forming a packing surface with different sets of atoms. Therefore, the Leu substitution for Gln 652 strengthens the interhelix interaction by providing additional hydrophobic packing forces and/or removing the burial of polar atoms. Moreover, the Q652L mutant peptide is a potent inhibitor of HIV-1 infection, with 10-fold greater activity than the wild-type peptide. This inhibitory potency correlates with the coiled-coil-binding potential of the corresponding C-terminal mutant peptide. Thus, the packing interactions of the six-helix bundle are likely to underlie the mechanism of membrane fusion. They also provide a good test-bed for developing more potent versions of C peptides.

MATERIALS AND METHODS

Mutagenesis and Peptide Production. Mutations were introduced into the N34(L6)C28 model by single-stranded mutagenesis (*35*) and verified by DNA sequencing. All recombinant peptides were expressed in *Escherichia coli* BL21(DE3) pLysS using the T7 expression system (*36*). Cells, freshly transformed with an appropriate plasmid, were grown to late log phase. Protein expression was induced by addition of 0.5 mM isopropylthio-β-D-galactoside (IPTG). After another 3 h of growth at 37 or 30 °C, the bacteria were harvested by centrifugation, and the cells were lysed by glacial acetic acid as described previously (*16*). Peptides were purified from the soluble fraction to homogeneity by reversed-phase high-performance liquid chromatography (HPLC), using a Vydac C-18 preparative column and a linear gradient of acetonitrile containing 0.1% trifluoroacetic acid. The C34 and C34/Q652L peptides were synthesized by solid-phase FMOC methods and purified by HPLC as described above. In each peptide, the N-terminus is acetylated and the C-terminus is amidated. Peptide identity was confirmed by mass spectrometry. Peptide concentrations were determined by absorbance at 280 nm in the presence of 6 M guanidinium hydrochloride (GdmCl) (*37*).

Circular Dichroism (CD) Spectroscopy. CD spectra were acquired at 10 μM peptide concentration in 50 mM sodium phosphate, pH 7.0, and 150 mM NaCl (PBS) with an Aviv 62 DS spectrometer as described previously (*38*). The wavelength dependence of molar ellipticity, $[\theta]$, was monitored at 0 or 20 °C as the average of five scans, using a five-second integration time at 1.0 nm wavelength increments. Spectra were baseline-corrected against the cuvette with buffer alone. Helix content was estimated from the CD signal by dividing the mean residue ellipticity at 222 nm by the value expected for 100% helix formation by helices of comparable size, −33 000 deg cm^2 dmol^{-1} (*39*). Thermal stability was determined by monitoring the change in CD signal at 222 nm as a function of temperature, and thermal melts were performed in two-degree intervals with a 2 min equilibration at the desired temperature and an integration time of 30 s. Reversibility was checked by repeated scans. The midpoint of the thermal unfolding transition (apparent T_m) was determined from the maximum of the first derivative, with respect to the reciprocal of the temperature, of the $[\theta]_{222}$ values (*40*). The error in estimation of T_m is ±0.5 °C.

Sedimentation Equilibrium. Sedimentation equilibrium analysis was performed on a Beckman XL-A analytical ultracentrifuge as described previously (*38*). Peptide solutions were dialyzed overnight against PBS, loaded at initial concentrations of 10, 30, and 100 μM, and analyzed at rotor speeds at 20 and 23 krpm at 20 °C. Data sets were fitted simultaneously to a single-species model with the program NONLIN (*41*). Protein partial specific volume and solvent density were calculated with constants from Laue et al. (*42*). Molecular weights were all within 10% of those calculated for an ideal trimer, with no systematic deviation of the residuals.

Crystallization, Data Collection, and Structure Determination. The Q652L variant was crystallized by the sitting drop vapor diffusion method at room temperature. To grow crystals, a 10 mg/mL HPLC-purified peptide stock was diluted 1:1 with a reservoir and allowed to equilibrate against the reservoir solution. Initial crystallization conditions were screened by using sparse matrix crystallization kits (Crystal Screen I and II, Hampton Research, Riverside, CA) and then optimized. Crystals of Q652L in space group $R3$ ($a = b =$ 52.38 Å, $c = 60.48$ Å) were grown from 0.2 M ammonium sulfate, 0.1 M sodium acetate, pH 4.6, and 11% poly(ethylene glycol) 4000 and transferred to a cryoprotected solution containing 15% (vol/vol) glycerol in the corresponding mother liquor. Data were collected at 95 K using an R-axis IV image plate detector mounted on a Rigaku RU200 rotating anode X-ray generator at the X-ray Crystallography Facility

Table 1: Summary of Circular Dichroism and Sedimentation Equilibrium Data for N34(L6)C28 Mutants

core model	$-[\theta]_{222}$ (deg cm^2 dmol^{-1})	T_m (°C)	T_m^{GdmCl} (°C)[a]	molecular mass (kDa)
N34(L6)C28	31 300	70	46	24.4
Q652L	31 900	72	48	24.9
Q652L/I573S	19 900	24		

[a] T_m^{GdmCl} denotes the melting temperature in 2 M GdmCl. All scans and melts were performed at 10 μM peptide concentration.

Table 2: X-ray Data Collection and Refinement Statistics

unit cell dimensions	
a, *b*, *c* (Å)	52.38, 52.38, 60.48
α, β, γ (deg)	90, 90, 120
space group	*R*3
data processing	
resolution (Å)	50.0−2.0
measured reflections	23 565
unique reflections	4167
completeness (%)	99.7
R_{merge}[a](%)	4.0
refinement	
resolution (Å)	50.0−2.0
reflections in working set	3668
reflections in test set	499
protein nonhydrogen atoms	510
water molecules	77
R_{free}[b] (%)	24.3
R_{cryst}[b] (%)	20.6
average *B*-factor (Å^2)	38.5
rms deviations from ideality	
bond lengths (Å)	0.005
bond angles (deg)	0.768
torsion angles (Å)	14.8

[a] $R_{merge} = \Sigma|I - \langle I\rangle|/\Sigma I$, where I is the intensity of an individual measurement and $\langle I\rangle$ is the average intensity from multiply recorded reflections. [b] $R_{cryst} = \Sigma|F_{obs} - F_{calc}|/\Sigma F_{obs}$, where F_{obs} and F_{calc} are observed and calculated structural factors, respectively. No σ-cutoff was applied. R_{free} is calculated for a set of reflections that were excluded from refinement.

at the Weill Medical College of Cornell University. Diffraction intensities were integrated by using DENZO and SCALEPACK software (*43*) and reduced to structural factors with the program TRUNCATE from the CCP4 program suite (*44*).

The structure of Q652L was determined by molecular replacement by using the program AMoRe (*45*). The 2.4 Å structure of wild-type N34(L6)C28 (PDB file name 1STZ) was used in a combined rotation-translation search (with 15.0−3.5 Å data) to yield a solution for Q652L (correlation coefficient = 66.1%; *R*-factor = 46.5%). The model was refined with simulated annealing and atomic displacement parameter (ADP) refinements using the program X-PLOR (*46*). Density interpretation and model building were done with the program O (*47*). Prior to refinement, 5% of the diffraction data were set aside for cross validation (free *R*-factor calculation). Crystallographic refinement of the structure was done with the program CNS 0.5 (*48*). The final refined model (R_{cryst} = 20.6%; R_{free} = 24.3%) includes 189−204 residues in the N34(L6)C28 trimer, and 77 water molecules (Table 2). Residues 546, 654, and 655 of gp41 and Gly 2 and Gly 3 of the linker were left out of the model because of the absence of interpretable electron density for these atoms. The Arg 579 side chain of gp41 and the Arg 4 side chain of the linker are disordered and were thus modeled as alanine.

Cell−Cell Fusion and Infectivity Assays. The inhibitory activities of N34(L6)C28 and variants thereof were determined by using a dye transfer fusion assay as described previously (*49*). HIV-1_{IIIB}-infected H9 cells were labeled with 2′,7′-bis-(2-carboxyethyl)-5-(and-6)-carboxyfluorescein-acetoxymethyl ester (BCECF-AM). Fluorescently labeled HIV-1_{IIIB}-infected H9 cells (1×10^4) and MT-2 cells were cocultured at 1:10 ratio at varying peptide concentrations for 2 h at 37 °C in a 96-well microplate to obtain a dose−response curve. The fused cells were scored for dye transfer under fluorescence microscopy. In the infectivity assay as described previously (*50*), HIV-1_{IIIB} was inoculated with 1×10^4 of MT-2 cells at 0.0045 multiplicity of infection in RPMI 1640 containing 10% fetal bovine serum in the presence of varying peptide concentrations. After incubation at 37 °C for 1 and 24 h, half of the culture media was changed. HIV-1_{IIIB} -mediated cytopathic effect (CPE) was assessed by viability assay 6 days after infection.

RESULTS

Solution Properties of Q652L. Genetic studies indicate that substituting leucine for a conserved glutamine (Gln 652) within the C-terminal helix of gp41 results in higher than wild-type membrane fusion activity (*25*). This enhanced fusion activity is unlikely to be due to higher protein expression because the wild-type and mutant envelope glycoproteins have similar cell-surface expression (*25*). The crystal structure of the gp41 ectodomain core revealed that the Gln 652 side chain packs into a highly conserved hydrophobic groove of the coiled coil and that the carboxyl group of Gln 652 forms a tertiary hydrogen bond with the amide of Asn 554 (*17*−*19*). To understand how the Gln 652 to Leu mutation affects the structure and stability of the six-helix bundle, we substituted Gln 652 with leucine in the recombinant N34(L6)C28 model, a system that retains many structural features characteristic of the fusion-active gp41 core (*19*, *21*). This mutant peptide was named Q652L.

The Q652L mutant peptide was produced by bacterial expression and purified to homogeneity by HPLC (see Materials and Methods). The circular dichroism spectrum of Q652L indicates that the folded mutant peptide contains greater than 95% α-helical structure (Figure 2a; Table 1). Sedimentation equilibrium measurements demonstrate that Q652L forms a clean trimer over a 10-fold range of peptide concentrations (10−100 μM) (Figure 2c; Table 1). These results indicate that, like the wild-type peptide, the Q652L mutant forms a six-helix bundle structure in solution. Thus, the Gln 652 to Leu mutation does not affect the overall protein fold of the gp41 core.

The stability of the Q652L mutant peptide was assessed by monitoring the change in $[\theta]_{222}$ as a function of temperature. In neutral pH phosphate-buffered saline (PBS) at 10 μM peptide concentration, the apparent melting temperature (T_m) of Q652L is 72 °C, relative to 70 °C for N34(L6)C28 (wild-type) (Table 1). Like the wild-type peptide, the thermally induced unfolding transition of the Q652L mutant is not reversible and the solution becomes turbid upon heat denaturation. In the presence of the denaturant guanidinium hydrochloride (GdmCl) at 1.5 M concentration, both the wild-type and mutant peptides undergo cooperative and reversible unfolding transitions, with T_ms of 54 and 56 °C,

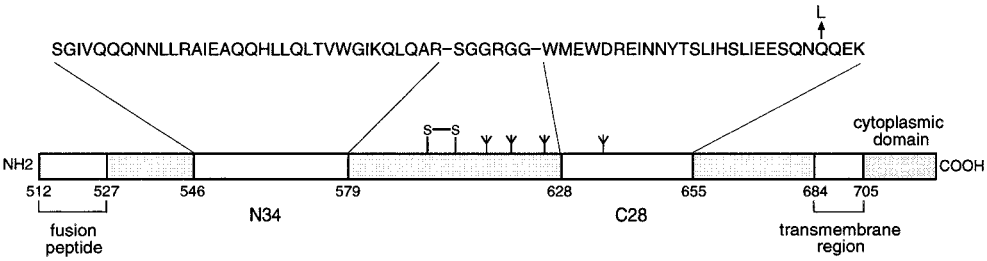

FIGURE 1: Schematic view of the HIV-1 gp41 envelope protein. The amino acid sequences of the N34 and C28 segments are shown. The N34(L6)C28 model of the gp41 ectodomain core consists of N34 and C28 plus a six-residue linker (*21*). A Gln 652 to Leu mutation that increases HIV-1 infectivity is indicated above the sequence. The disulfide bond and four potential N-glycosylation sites are depicted. The residues are numbered according to their position in gp160.

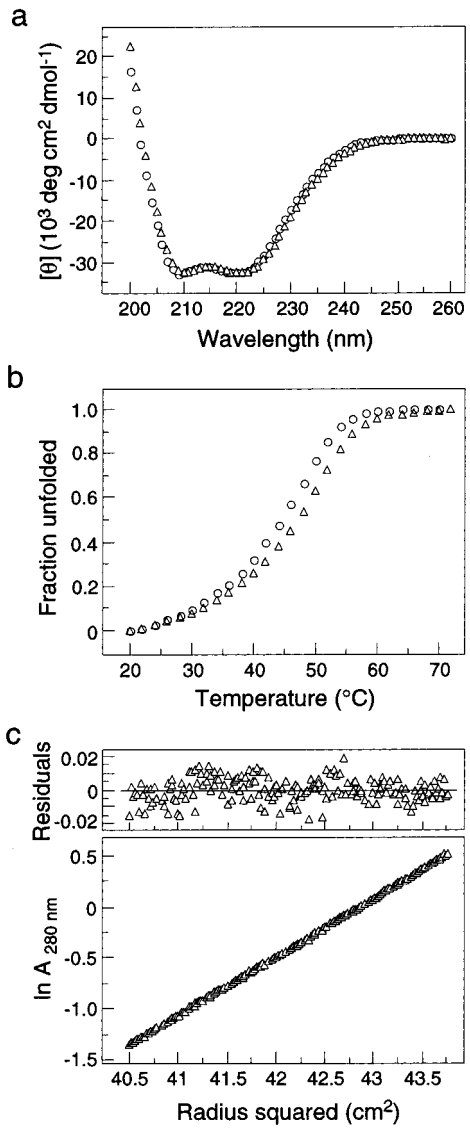

FIGURE 2: Folding of Q652L into a stable α-helical trimer. (a) Circular dichroism (CD) spectra of wild-type N34(L6)C28 (circles) and Q652L (triangles) at 0 °C in PBS (pH 7.0). (b) Thermal melts of N34(L6)C28 (circles) and Q652L (triangles) monitored by CD at 222 nm at 10 μM peptide concentration in PBS (pH 7.0) in the presence of 2 M GdmCl. The decrease in the fraction of a folded molecule is shown as a function of temperature. (c) Analytical ultracentrifugation data (20 krpm) for Q652L collected at 20 °C in PBS (pH 7.0) at ~30 μM peptide concentration. The natural logarithm of the absorbance at 280 nm is plotted against the square of the radial position. Deviations from the calculated values are plotted as residuals (top portion of panel c).

respectively (Figure 2b; Table 1). The change in thermal stability, ΔT_m, between the wild-type and mutant peptides is 2 °C in the presence and absence of GdmCl. By using the Gibbs−Helmholtz equation, together with the thermodynamic parameters determined for the SIV N34(L6)C28 peptide (I. Jelesarov, H. R. Bosshard, H. J., and M. L., unpublished data), the corresponding free energy difference is -0.8 ± 0.3 kcal/mol for Q652L, relative to the wild-type peptide. Thus, the six-helix bundle structure of the gp41 core is stabilized by the Gln 652 to leucine substitution.

Crystal Structure of Q652L. To investigate the basis for the enhanced stability of the mutant molecule, the X-ray crystal structure of the Q652L peptide was determined to 2.0 Å resolution using the molecular replacement method. The final $2F_o - F_c$ electron density map is of good quality (see Figure 3) and reveals the positions of all the amino acid residues except four at the helix termini and in the linker region (Figure 4a). Omit maps were calculated to confirm the assignment of the side chains. The structure of Q652L was refined to a conventional *R*-factor of 20.6% with a free *R*-factor of 24.3% and root-mean-square deviations from ideal bond lengths and bond angles of 0.005 Å and 0.768°, respectively (Table 2). The quality of the refined model was checked by PROCHECK (*51*). All main-chain torsional angles fall within the helical region of a Ramachandran plot. Details of the data collection and refinement statistics are given in Table 2.

Like the wild-type peptide, the Q652L mutant folds into a six-helix bundle composed of three helical hairpins, each consisting of an N34 helix paired with an antiparallel C28 helix (Figure 4a). At the center of the bundle, the side chains at the heptad ***a*** and ***d*** positions of the N34 coiled coil displays typical "knobs-into-holes" packing interactions (*52*, *53*). Three C28 helices wrap in the reverse direction against the outside of the N34 coiled-coil trimer and are tilted relative to the N34 superhelix by approximately 13° (Figure 4b). These C28 helices interact with the N34 helices through residues in three highly conserved hydrophobic grooves on the surface of the coiled-coil trimer (Figure 4c). In general, residues in the ***a*** and ***d*** positions of the C28 helix pack against residues at the ***e*** and ***g*** positions of the N34 helices. The root-mean-square (rms) deviation between all C_α atoms of the central N34 coiled coil in the wild-type and mutant molecules is 1.14 Å. The C28 helices in Q652L can also be superimposed upon the wild-type counterpart with a rms deviation of 1.52 Å. Thus, the overall architecture and helix packing of the Q652L mutant are the same as that of the wild-type molecule.

Although most of the helix packing interface within the gp41 core structure involves hydrophobic interactions, interhelical hydrogen bonds and salt bridges are uniformly

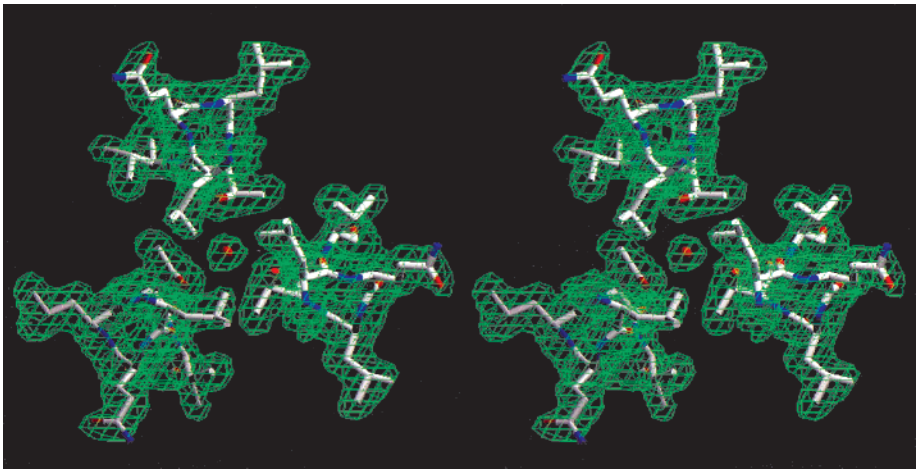

FIGURE 3: Stereoview of the final $2F_o - F_c$ electron-density map of the Q652L mutant with the refined model superimposed. Oxygen, nitrogen, and carbon atoms are colored red, blue, and white, respectively. A water molecule within the central N34 coiled coil of Q652L is shown as red balls. The map is contoured at 1.0 standard deviation above the average density. Figure was generated by using the program SETOR (*66*).

Table 3: Inhibitory Potency of gp41 Peptides

peptide	IC_{50} (nM)	
	cell-cell fusion[a]	HIV-infectivity[b]
N34(L6)C28	1508 ± 160	1487 ± 87
Q652L	180 ± 25	116 ± 12
Q652L/I573S	208 ± 17	308 ± 30
I573S	685 ± 9	730 ± 20
C28	947 ± 67	2,192 ± 19
C34	29.8 ± 1.7	17.2 ± 1.6
C34/Q652L	7.4 ± 0.7	6.8 ± 0.3

[a] Inhibition of cell−cell fusion was measured in a syncytium formation. Indicated is the mean and standard deviation ($n = 4$). [b] Inhibition of HIV-1 infectivity was measured in a cell-culture infection assay. Indicated is the mean and standard deviation ($n = 3$).

distributed along the hydrophobic contacts. In the wild-type structure, a cluster of polar glutamines, including Gln 652, is involved in an intricate network of interhelical hydrogen bonds; a conserved salt bridge is formed between Asn 554 from N34 and Gln 652 from C28 in the wild-type structure (Figure 5). The substituted Leu 652 side chain forms a well-packed interface that lacks an interhelical hydrogen bond (Figure 5). The distances between the Leu 652 C_β atom and the symmetry-related C_β atoms of Gln 550 and Gln 551 from the N34 helix are 6.17 and 4.68 Å, respectively. In contrast, the corresponding distances for the wild-type Gln 652 side chain are 6.50 Å for Gln 550 and 5.73 Å for Gln 551. These favorable van der Waals interactions in the Q652L mutant appear to strengthen helix−helix packing and stabilize the six-helix bundle structure. In addition, the Gln 652 to Leu substitution also leads to local structural rearrangements; the side chains of Asn 553, Trp 628, and Gln 653 deviates substantially (Figure 4, panels b and c). These side chains may be poorly ordered due to chain termini effects or on the surface of the bundle. Overall, the nonpolar Leu 652 side chain makes good interhelical packing interactions and is well accommodated without significantly altering the six-helix bundle structure.

Antiviral Activity of Q652L. Synthetic peptides that make up the gp41 core are potent inhibitors of HIV infection and syncytium formation (*49*, *54*, *55*). We have previously shown that the N34(L6)C28 peptide itself inhibits HIV-1-mediated membrane fusion at micromolar concentrations (*21*). To examine whether the fusion-enhanced Gln 652 to leucine mutation affects the antiviral activity of N34(L6)C28, we determined the relative potencies of the wild-type and mutant peptides to inhibit HIV-1 infection using both cell−cell fusion and infectivities assays. Figure 6 shows the inhibition of HIV-1_{IIIB}-infected H9 cell-mediated syncytium formation and cytopathic effect by different concentrations of peptides. Interestingly, the Q652L peptide is a highly effective inhibitor, with 50% inhibition concentrations (IC_{50}) of 0.18 μM for syncytium formation and 0.12 μM for viral entry, compared with IC_{50} values of 1.51 and 1.49 μM for the wild-type N34(L6)C28 peptide (Figure 6; Table 3). Thus, the Gln 652 to leucine mutation increases the inhibitory activity of N34(L6)C28 about 10-fold.

To test if the six-helix bundle structure is required for the enhanced antiviral activity of the mutant peptide, we substituted Ile 573, an ***a*** heptad position, with Ser in Q652L to produce the double mutant Q652L/I573S. The Ile 573 to Ser mutation was chosen because it essentially disrupts the six-helix complex formation (*21*). Circular dichroism experiments confirm that this double mutant contains ~60% helical structure, with an apparent T_m of 24 °C (Figure 7a; Table 1). The Q652L/I573S peptide inhibits cell−cell fusion and infection with IC_{50}s of 0.21 and 0.31 μM, respectively, compared with IC_{50} values of 0.69 and 0.73 μM for the single I573S mutant (Figure 7b; Table 3). In addition, the isolated C28 peptide blocks syncytium formation and viral entry with IC_{50} values of 0.95 and 2.19 μM (Table 3). Taken together, these results strongly suggest that the enhanced antiviral activity of the Q652L peptide, relative to the wild-type molecule, results from the unfolded C28 segment bearing the Gln 652 to Leu mutation.

To further clarify this relationship, synthetic peptides with blocked termini, corresponding to the C34 sequence and its variant containing the Gln 652 to Leu mutation, were generated. The C34 peptide identified by the protein dissection method spans residues 628−661 and contains the entire region of the C28 peptide (*16*). C34 was chosen because this 34-residue peptide is soluble in aqueous solution and has high inhibitory activity (*16*, *26*). Whereas wild-type C34 showed IC_{50} values of 29.8 and 17.2 nM for inhibition of syncytium formation and HIV-1 entry, respectively, the

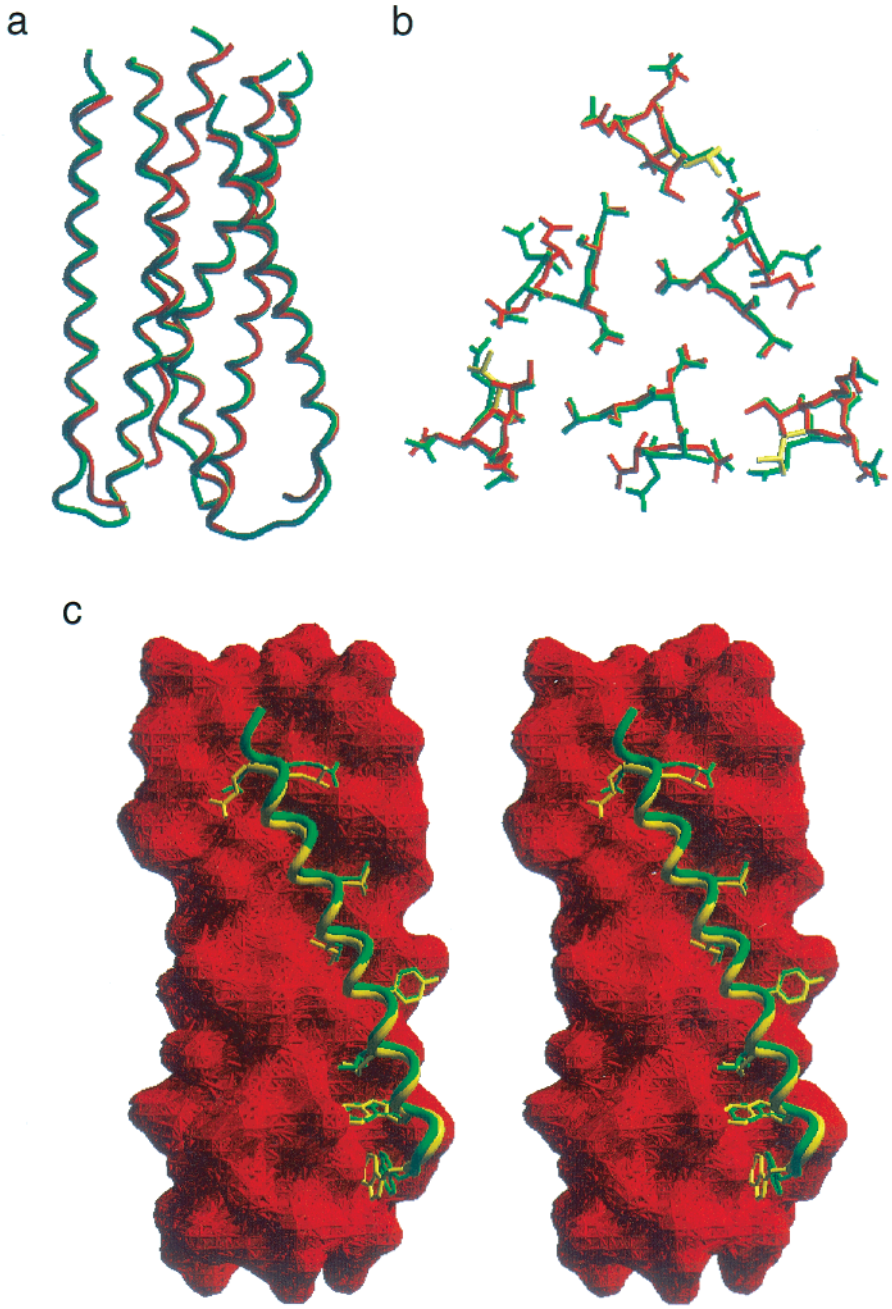

FIGURE 4: X-ray crystal structure of the Q652L mutant gp41 core. (a) Side view. The alpha-carbon traces of the N34 and C28 helices in the wild-type N34(L6)C28 (green) and mutant Q652L (red) structures were used for the superposition. The amino terminus of N34 and the carboxyl terminus of C28 are at the top of the figure. (b) A cross-section of the helix packing near the Gln 652 residue. Structures of wild-type N34(L6)C28 (green) and Q652L (red) are overlaid. The side chain of the mutated Gln 652 residue is colored yellow. (c) Stereoview of the interaction of the C28 helix with the conserved hydrophobic groove on the surface of the N34 coiled coil in the Q652L mutant gp41 core. The C28 helices of wild-type N34(L6)C28 (green) and Q652L (yellow), represented as ribbons, are shown against a surface representation of the central N34 coiled coil in wild-type N34(L6)C28. Figures were generated with the program SETOR (*66*).

IC_{50} of C34/Q652L is 7.4 nM for syncytium formation and 6.8 nM for viral entry (Figure 8; Table 3). Thus, the Gln 652 to leucine mutation resulted in a ~2.5−4-fold increase in inhibitory activity.

DISCUSSION

The structure and mechanism of the HIV-1 envelope glycoprotein have been studied intensively. It has been shown that binding of gp120 to cell-surface receptors activates the membrane fusion activity of gp41, which then mediates membrane fusion (reviewed in ref *3*). By analogy with the low-pH-induced structural changes in the influenza virus hemagglutinin (HA) protein, this fusion activation process likely involves a substantial conformational change in the gp120−gp41 complex that switches from a labile native structure to an energetically more stable and fusogenic conformation (*9*, *10*, *28*, *56*−*59*). The native gp120−gp41 structure is thought to be substantially different from that present in the fusogenic conformation, as has been established for the case of influenza HA (*10*, *60*). Although little is known about the details of the receptor-activated conformational change in the HIV-1 envelope protein, the soluble ectodomain of gp41 is well characterized. The core structure of this ectodomain is a six-helix bundle (*17*−*19*, *61*). Several

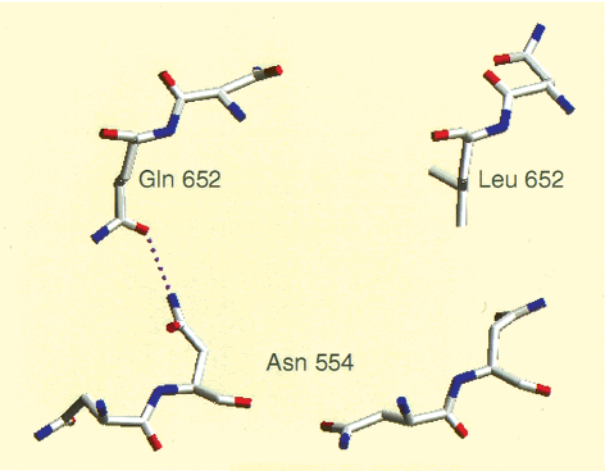

FIGURE 5: Side-chain carbonyl group of Gln 652 forms a tertiary hydrogen bond with the side-chain amide of Asn 554 in the wild-type structure (left panel). This hydrogen bond is not formed in the mutant Q652L structure (right panel). Oxygen, nitrogen, and carbon atoms are colored red, blue, and white, respectively. Hydrogen bond is shown in a purple dotted line. Figure was created with the program SETOR (*66*).

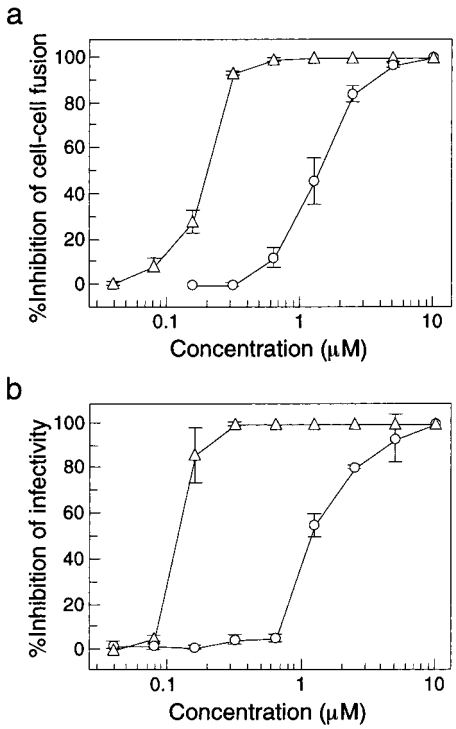

FIGURE 6: Inhibitory potency of the mutant Q652L peptide. (a) Inhibition of HIV-1_{IIIB}-infected H9 cell-induced cell−cell fusion by wild-type N34(L6)C28 (circles) and Q652L (triangles). Error bars indicate standard deviations from quadruplicate experiments. (b) Inhibition of HIV-1_{IIIB}-mediated cytopathic effect by wild-type N34(L6)C28 (circles) and Q652L (triangles). Error bars indicate standard deviations form triplicate experiments.

independent lines of evidence suggest that this structure corresponds to the fusogenic conformation of gp41 (*15*, *17*−*20*, *24*, *26*, *27*, *30*, *32*). Given that the fusion peptide region, which lies on the top of the N-terminal coiled coil, inserts into the cell membrane and the transmembrane helix at the C-terminus of the ectodomain is embedded in the viral membrane, the role of the six-helix bundle structure is proposed to facilitate the apposition of the viral and cellular membranes for fusion (*6*, *18*, *23*, *24*). While few details are

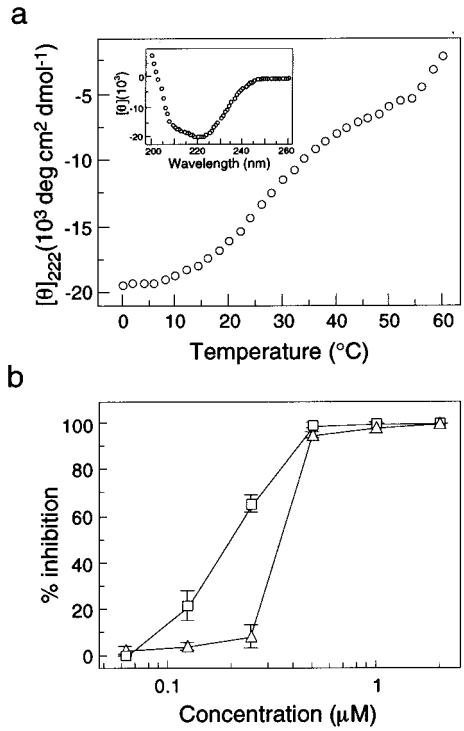

FIGURE 7: Ile 573 to Ser substitution in the Q652L mutant peptide disrupts the six-helix bundle formation and retains its potent inhibitory activity. (a) Thermal melt of Q652L/I573S monitored by CD at 222 nm. (Inset) CD spectrum at 0 °C at 10 μM peptide concentration in PBS (pH 7.0). (b) Inhibition of HIV-1_{IIIB}-infected H9 cell-induced cell−cell fusion (circles) and HIV-1_{IIIB}-mediated cytopathic effect (squares) by Q652L/I573S. Error bars indicate standard deviations from quadruplicate and triplicate experiments for cell−cell fusion and CPE, respectively.

known about how this membrane juxtaposition leads to complete membrane fusion, it is widely believed that the fusion involves the higher-order assembly of envelope protein trimers to form fusion pores (*62*).

Mutagenesis studies indicate that the packing interactions between the N- and C-terminal helices of gp41 are critical for HIV-1 membrane fusion. The conserved Gln 652 and Asn 656 residues on the buried face of the C-terminal helix are packed into a hydrophobic groove on the N-terminal coiled-coil surface within the gp41 core structure (*17*−*19*, *61*). Whereas the Asn 656 to Leu mutation abolishes HIV-1 infectivity, the Gln 652 to Leu mutation enhances membrane fusion activity (*25*). Our X-ray crystallographic data indicate that this fusion-enhancement mutation sequence is well accommodated in the six-helix bundle structure by forming a packing surface with different sets of atoms. The crystal structures of the wild-type and mutant molecules can be superimposed, with a rms deviation of 1.40 Å. The free energy of helical interface stabilization associated with the Gln 652 to Leu mutation in the mutant structure is −0.8 kcal/mol, as determined by thermal unfolding studies. The enhanced membrane fusion activity by this mutation correlates with structural perturbations that strengthen helical-packing interactions within the six-helix bundle. Our results provide strong evidence that the helical-packing rearrangements triggered by receptor binding are likely to underlie the mechanism of the gp41 conformational change required for activation of HIV-1 membrane fusion. Interestingly, a similar mechanism is also proposed for many other viral membrane fusion proteins as well as the SNARE proteins

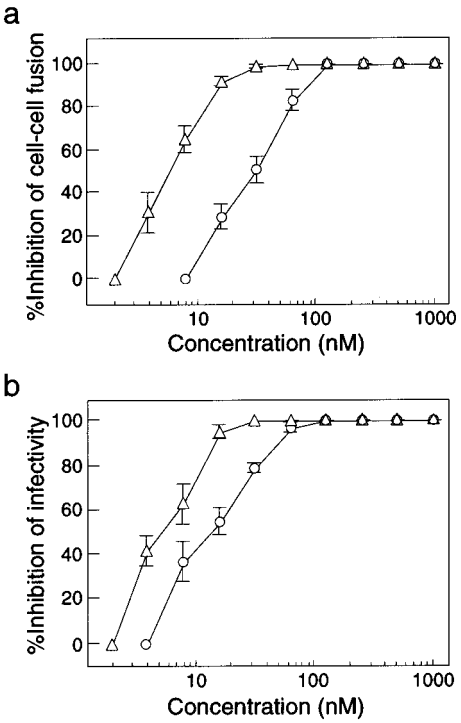

FIGURE 8: Inhibitory potency of the C34 and C34/Q652L peptides. (a) Inhibition of HIV-1_{IIIB}-infected H9 cell-induced cell−cell fusion by C34 (circles) and C34/Q652L (triangles). Error bars indicate standard deviations from quadruplicate experiments. (b) Inhibition of HIV-1_{IIIB}-mediated cytopathic effect by C34 (circles) and C34/Q652L (triangles). Error bars indicate standard deviations form triplicate experiments.

that mediate cellular membrane fusion processes (for a recent review, see ref *63*).

Peptides corresponding to the N- and C-terminal heptad-repeat regions of gp41 are themselves effective inhibitors, at micromolar to nanomolar concentrations, of HIV-1 infection and syncytium formation (*15*, *49*, *54*, *55*). Peptides from the C-terminal region of the ectodomain have the highest activity. It is striking that these peptides are effective against both laboratory-adapted strains and primary isolates of HIV-1 (*49*, *54*, *55*). The C peptide T-20 shows high efficacy in reducing viral loads in clinical trials (*64*). A large body of data is consistent with the proposal that these peptide inhibitors work through a dominant-negative mechanism by binding to viral gp41 and leading to its inactivation (*15*, *17*−*19*, *24*, *26*−*32*). Kinetic studies demonstrate that the T-20 peptide does not act on the native gp120−gp41 complex but binds to gp41 only after interaction of the envelope complex with its cellular receptor (CD4) and coreceptors (e.g., CCR5 or CXCR4), suggesting strongly that the trimeric coiled coil of gp41 is available transiently during the conformational change to the fuogenic state (*24*). In addition, the conserved hydrophobic cavity on the gp41 coiled coil that provides a binding pocket for conserved C-peptide residues is proposed to be a good drug target for the development of small-molecule inhibitors of HIV-1 infection (*26*).

The N34(L6)C28 peptide model of the gp41 core is also capable of blocking HIV-1 membrane fusion at micromolar concentrations (*21*). Given that this inhibitory activity cannot be traced to the dissociated C28 region of the molecule, a mechanism different from that in the dominant-negative model proposed for the isolated N and C peptides is probably involved in the inhibition of membrane fusion by the N34(L6)C28 complex (*21*). The inhibitory potency of N34(L6)C28 is dramatically increased by the fusion-defective Leu 568 to Ala and Trp 571 to Arg mutations that introduce structural perturbations in the coiled-coil cavity and thus weaken inter-helical packing interactions within the gp41 core (*25*, *27*). This enhanced inhibitory activity is likely to result from the synergistic inhibition of the N34 and C28 peptides in the mutant molecules (*27*).

In this study, we demonstrate that the Gln 652 to Leu mutation also exerts striking effects on the inhibitory potency of N34(L6)C28; the Q652L mutant exhibits ∼10-fold greater activity than the wild-type peptide. We also demonstrate that this enhanced inhibitory activity is likely to reflect that of the corresponding mutant C28 segment. Thus, the Gln 652 to Leu mutation can impart strong helical character and binding energy to the C28 peptide for binding to the trimeric coiled coil of gp41, as predicted by a dominant-negative mode of inhibition. Our data further show that the Gln 652 to Leu substitution can render the synthetic C34 peptide ∼3-fold greater activity. Since this increase in inhibitory potency is less dramatic than that seen in the N34(L6)C28 variant, it is possible that more than one mechanism is responsible for the enhanced inhibitory activity of the Q652L peptide. Further studies are needed to ascertain the mechanism by which the six-helix bundle blocks viral fusion with host cells.

Overall, our results indicate that the conserved interhelical packing interactions within the six-helix bundle structure of gp41 play a role in HIV-1 entry and its inhibition. It remains to be determined whether these interactions underlie the mechanism for the proposed gp41 conformational change during fusion activation (*6*, *18*, *23*, *24*; see, however, ref *61*). Because the interhelical interactions have been shown to account for the broad antiviral activity of C peptides (*55*, *65*), our results suggest that more potent analogues of C peptide inhibitors can be tested for the ability to form a stable complex with the N-terminal coiled coil of gp41.

REFERENCES

1. Turner, B. G., and Summers, M. F. (1998) *J. Mol. Biol. 285*, 1−32.
2. Luciw, P. A. (1996) in *Fields Virology* (Fields, B. N., Knipe, D. M., Howley, P. M., Chanock, R. M., Melinick, J. L., Monath, T. P., Roizman, B., and Straus, S. E., Eds.) pp 1881−1952, Lippincott-Raven Publishers, Philadelphia.
3. Moore, J. P., Jameson, B. A., Weiss, R. A., and Sattentau, Q. J. (1993) in *Viral Fusion Mechanisms* (Bentz, J., Ed.) pp 233−289, CRC Press, Boca Raton.
4. Kwong, P. D., Wyatt, R., Robinson, J., Sweet, R. W., Sodroski, J., and Hendrickson, W. A. (1998) *Nature 393*, 648−659.
5. Rizzuto, C. D., Wyatt, R., Hernandez-Ramos, N., Sun, Y., Kwong, P. D., Hendrickson, W. A., and Sodroski, J. (1988) *Science 280*, 1949−1953.
6. Chan, D. C., and Kim, P. S. (1998) *Cell 93*, 681−684.
7. Stegmann, T., Delfino, J. M., Richards, F. M., and Helenius, A. (1991) *J. Biol. Chem. 266*, 18404−18410.
8. Tsurudome, M., Gluck, R., Graf, R., Falchetto, R., Schaller, U., and Brunner, J. (1992) *J. Biol. Chem. 267*, 20225−20232.
9. Carr, C. M., and Kim, P. S. (1993) *Cell 73*, 823−832.
10. Bullough, P. A., Hughson, F. M., Skehel, J. J., and Wiley, D. C. (1994) *Nature 371*, 37−43.
11. Hernandez, L. D., Hoffman, L. R., Wolfsberg, T. G., and White, J. M. (1996) *Annu. Rev. Cell Dev. Biol. 12*, 627−661.
12. Chambers, P., Pringle, C. R., and Easton, A. J. (1990) *J. Gen. Virol. 71*, 3075−3080.

13. Delwart, E. J., Mosialos, G., and Gilmore, T. (1990) *AIDS Res. Hum. Retroviruses 6*, 703−706.
14. Gallaher, W. R., Ball, J. M., Garry, R. F., Griffin, M. C., and Montelaro, R. C. (1989) *AIDS Res. Hum. Retroviruses 5*, 431−440.
15. Lu, M., Blacklow, S. C., and Kim, P. S. (1995) *Nat. Struct. Biol. 2*, 1075−1082.
16. Lu, M., and Kim, P. S. (1997) *J. Biomol. Struct. Dyn. 15*, 465−471.
17. Chan, D. C., Fass, D., Berger, J. M., and Kim, P. S. (1997) *Cell 89*, 263−273.
18. Weissenhorn, W., Dessen, A., Harrison, S. C., Skehel, J. J., and Wiley, D. C. (1997) *Nature 387*, 426−430.
19. Tan, K., Liu, J., Wang, J., Shen, S., and Lu, M. (1997) *Proc. Natl. Acad. Sci. U.S.A. 94*, 12303−12308.
20. Jiang, S., Lin, K., and Lu, M. (1998) *J. Virol. 72*, 10213−10217.
21. Lu, M., Ji, H., and Shen, S. (1999) *J. Virol. 73*, 4433−4438.
22. Dubay, J. W., Roberts, S. J., Brody, B., and Hunter, E. (1992) *J. Virol. 66*, 4748−4756.
23. Hughson, F. M. (1997) *Curr. Biol. 7*, R565−R569.
24. Furuta, R. A., Wild, C. T., Weng, Y., and Weiss, C. D. (1998) *Nat. Struct. Biol. 5*, 276−279.
25. Cao, J., Bergeron, L., Helseth, E., Thali, M., Repke, H., and Sodroski, J. (1993) *J. Virol. 67*, 2747−2755.
26. Chan, D. C., Chutkowski, C. T., and Kim, P. S. (1998) *Proc. Natl. Acad. Sci. U.S.A. 95*, 15613−15617.
27. Ji, H., Shu, W., Burling, F. T., Jiang, S., and Lu, M. (1999) *J. Virol. 73*, 8578−8586.
28. Chen, C. H., Matthews, T. J., McDanal, C. B., Bolognesi, D. P., and Greenberg, M. L. (1995) *J. Virol. 69*, 3771−3777.
29. Wild, C. T., Greenwell, T., Shugars, D., Rimsky-Clarke, L., and Matthews, T. (1995) *AIDS Res. Hum. Retroviruses 11*, 323−325.
30. Judice, J. K., Tom, J. Y. K., Huang, W., Wrin, T., Vennari, J., Petropoulos, C. J., and McDowell, R. S. (1997) *Proc. Natl. Acad. Sci. U.S.A. 94*, 13426−13430.
31. Rimsky, L. T., Shugars, D. C., and Matthews, T. J. (1998) *J. Virol. 72*, 986−993.
32. Munoz-Barroso, I., Durell, S., Sakaguchi, K., Appella, E., and Blumenthal, R. (1998) *J. Cell Biol. 140*, 315−323.
33. Weissenhorn, W., Carfi, A., Lee, K.-H., Skehel, J. J., and Wiley, D. C. (1998) *Mol. Cell 2*, 605−616.
34. Malashkevich, V. N., Schneider, B. J., McNally, M. L., Milhollen, M. A., Pang, J. X., and Kim, P. S. (1999) *Proc. Natl. Acad. Sci. U.S.A. 96*, 2662−2667.
35. Kunkel, T. A., Roberts, J. D., and Zakour, R. A. (1987) *Methods Enzymol. 154*, 367−382.
36. Studier, F. W., Rosenberg, A. H., Dunn, J. J., and Dubendorff, J. W. (1990) *Meth. Enzymol. 185*, 60−89.
37. Edelhoch, H. (1967) *Biochemistry 6*, 1948−1954.
38. Shu, W., Ji, H., and Lu, M. (1999) *Biochemistry 38*, 5378−5385.
39. Chen, Y. H., Yang, J. T., and Chau, K. H. (1974) *Biochemistry 13*, 3350−3359.
40. Cantor, C., and Schimmel, P. (1980) *Biophysical Chemistry*, Part III, pp 1131−1132, W. H. Freeman and Company, New York.
41. Johnson, M. L., Correia, J. J., Yphantis, D. A., and Halvorson, H. R. (1981) *Biophys. J. 36*, 575−588.
42. Laue, T. M., Shah, B. D., Ridgeway, T. M., and Pelletier, S. L. (1992) in *Analytical Ultracentrifugation in Biochemistry and Polymer Science* (Harding, S. E., Rowe, A. J., and Horton, J. C., Eds.) pp 90−125, Royal Society of Chemistry, Cambridge.
43. Otwinowski, Z., and Minor, W. (1996) *Methods Enzymol. 276*, 307−326.
44. CCP4 (1994) *Acta Crystallogr., Sect. D 50*, 760−763.
45. Navaza, J. (1994) *Acta Crystallogr., Sect. A 50*, 157−163.
46. Brünger, A. T. (1992) *X-PLOR Version 3.1: A system for X-ray Crystallography and NMR*, Yale University Press, New Haven, CT.
47. Jones, T. A., Zou, J.-Y., and Cowan, S. W. (1991) *Acta Crystallogr., Sect. A 47*, 110−119.
48. Brünger, A. T., Adams, P. D., Clore, G. M., DeLano, W. L., Gros, P., Grosse-Kunstleve, R. W., Jiang, J.-S., Kuszewski, J., Nilges, M., Pannu, N. S., Read, R. J., Rice, L. M., Simonson, T., and Warren, G. L. (1998) *Acta Crystallogr., Sect. D 54*, 905−921.
49. Jiang, S., Lin, K., Strick, N., and Neurath, A. R. (1993) *Nature 365*, 113.
50. Jiang, S., Lin, K., and Neurath, A. R. (1991) *J. Exp. Med. 174*, 1557−1563.
51. Laskowski, R. A., MacArthur, M. V., Moss, D. D., and Thornton, J. M. (1993) *J. Appl. Crystallogr. 26*, 283−291.
52. Crick, F. H. C. (1953) *Acta Crystallogr. 6*, 689−697.
53. Harbury, P. B., Zhang, T., Kim, P. S., and Alber, T. (1993) *Science 262*, 1401−1407.
54. Wild, C. T., Oas, T., McDanal, C. B., Bolognesi, D., and Matthews, T. J. (1992) *Proc. Natl. Acad. Sci. U.S.A. 89*, 10537−10541.
55. Wild, C. T., Shugars, D. C., Greenwell, T. K. McDanal, C. B., and Matthews, T. J. (1994) *Proc. Natl. Acad. Sci. U.S.A. 91*, 9770−9774.
56. Carr, C. M., Chaudhry, C., and Kim, P. S. (1997) *Proc. Natl. Acad. Sci. U.S.A. 94*, 14306−14313.
57. Stegmann, T., and Helenius, A. (1993) in *Viral Fusion Mechanisms* (Bentz, J., Ed.) pp 233−289, CRC Press, Boca Raton.
58. Wiley, D. C., and Skehel, J. J. (1987) *Annu. Rev. Biochem. 56*, 365−394.
59. Chen, J., Wharton, S. A., Weissenhorn, W., Calder, L. J., Hughson, F. M., Skehel, J. J., and Wiley, D. C. (1995) *Proc. Natl. Acad. Sci. U.S.A. 92*, 12205−12209.
60. Wilson, I. A., Skehel, J. J., and Wiley, D. C. (1981) *Nature 289*, 366−373.
61. Caffrey, M., Cai, M., Kaufman, J. Stahl, S. J., Wingfield, P. T., Covell, D. G., Gronenborn, A. M., and Clore, G. M. (1998) *EMBO J. 17*, 4572−4584.
62. White, J. M. (1992) *Science 258*, 917−924.
63. Skehel, J. J., and Wiley, D. C. (1998) *Cell 95*, 871−874.
64. Kilby, J. M., Hopkins, S., Venetta, T. M., DiMassimo, B., Cloud, G. A., Lee, J. Y., Alldredge, Y., Hunter, E., Lambert, D., Bolognesi, D., Matthews, T., Johnson, M. R., Nowak, M. A., Shaw, G. M., and Saag, M. S. (1998) *Nat. Med. 4*, 1302−1307.
65. Malaskkevich, V. N., Chan, D. C., Chutkowski, C. T., and Kim, P. S. (1998) *Proc. Natl. Acad. Sci. U.S.A. 95*, 9134−9139.
66. Evans, S. V. (1993) *J. Mol. Graphics 11*, 134−138.

BI9921687